

## Chapter 1

### Radio Detection of High Energy Neutrinos

Amy L. Connolly

*Ohio State University, Department of Physics and CCAPP, Columbus, OH 43210  
USA*

Abigail G. Vieregg

*University of Chicago, Department of Physics, Enrico Fermi Institute, Kavli  
Institute for Cosmological Physics, Chicago, IL 60637 USA*

#### 1. Introduction

Ultra-high energy (UHE) neutrino astrophysics sits at the crossroads of particle physics, astronomy, and astrophysics.<sup>a</sup> Through neutrino astrophysics, we can uniquely explore the structure and evolution of the universe at the highest energies at cosmic distances and test our understanding of particle physics at energies greater than those available at particle colliders.

The detection of UHE neutrinos would shed light on the nature of the astrophysical sources that produce the highest energy particles in the universe. Astrophysical sources almost certainly produce UHE neutrinos in hadronic processes. Also, neutrinos above  $10^{17}$  eV should be produced through the GZK effect,<sup>1,2</sup> where extragalactic cosmic rays above  $10^{19.5}$  eV interact with the cosmic microwave background within tens of Mpc of their source. It was first pointed out by Berezhinsky and Zatsepin<sup>3,4</sup> that this cosmogenic neutrino flux, sometimes called “BZ” neutrinos, could be observable. These neutrinos would point close to the cosmic ray production site both because of the close proximity of the interaction to the source and because the decay products are Lorentz boosted along the line of sight. The latter effect constrains the direction the most strongly ( $1 \text{ MeV}/1 \text{ EeV} = 10^{-12}$  whereas  $100 \text{ Mpc}/1 \text{ Gpc} = 0.1$ ). Since cosmic rays do not follow straight paths in magnetic fields and get attenuated above the GZK threshold, and high energy photons ( $E > 10^{14}$  eV) are attenuated by the cosmic infrared background, neutrinos offer the unique ability to point to the location of the highest energy cosmic accelerators in

<sup>a</sup>Here, we loosely define the UHE regime to be the energy range near  $10^{18} - 10^{21}$  eV. A few radio experiments have sensitivities that reach to lower energies, while others have energy thresholds at higher energies.

the sky.

UHE neutrino measurements will also have important implications for high energy particle physics and determining neutrino properties. A sample of UHE neutrinos would allow for a measurement of the  $\nu$ -p cross section<sup>5,6</sup> and a direct test of weak interaction couplings at center-of-mass (CM) energies beyond the Large Hadron Collider (a  $10^{18}$  eV neutrino collides with a proton at rest at 45 TeV CM). A strong constraint on the UHE neutrino flux can even shed light on models of Lorentz invariance violation.<sup>7,8</sup>

IceCube has recently discovered neutrinos with energies up to a few  $10^{15}$  eV that are likely produced by astrophysical sources directly.<sup>9,10</sup> Therefore, there is now a pressing motivation to measure the energy spectrum above  $10^{15}$  eV with improved sensitivity, to provide insight into the origin of the seemingly cosmic events and the particle acceleration mechanisms that give rise to them and to determine the high-energy extent of the spectrum.

Figure 1 shows the current best limits on the high energy diffuse neutrino flux compared with a variety of GZK production models. Beyond the astrophysical neutrino events measured up to  $\sim 10^{15}$  eV, IceCube sets the best limits on the high energy neutrino flux up to  $10^{17.5}$  eV, and now shares the claim for the best constraints in the region up to  $10^{19.5}$  eV with the Pierre Auger Observatory (Auger).<sup>13,17</sup> The current best limit on the flux of neutrinos above  $10^{19.5}$  eV comes from the Antarctic Impulsive Transient Antenna (ANITA) experiment.<sup>15,16</sup>

Note that on the vertical axis of Figure 1 is the differential flux  $dN/dE$  multiplied by one power of  $E$ ; the product is proportional to  $dN/d\log_{10} E$ . On this plot, an experiment that increases its sensitivity in an

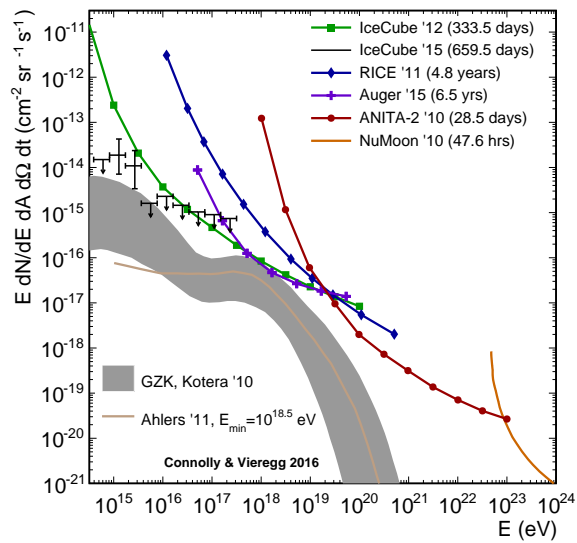


Fig. 1.: The current most competitive experimental constraints on the all-flavor diffuse flux of the highest energy neutrinos compared to representative model predictions.<sup>11,12</sup> Limits are from IceCube, Auger, RICE, ANITA and NuMoon.<sup>13–18</sup> Also shown is the astrophysical neutrino flux measured by IceCube.<sup>17</sup>

energy-independent way, for example by increasing its live time, will have its limits move only downward. An experiment that decreases its energy threshold with no other change will have its constraints move only to the left on this plot.

Despite the competitive limits currently imposed by optical detection experiments, it would be prohibitively costly to build a detector utilizing the optical signature that would be sensitive to the full range of predicted possible cosmogenic neutrino populations above  $10^{17}$  eV, due to the detector spacings set by the absorption and scattering lengths of optical light in ice.<sup>19</sup> IceCube-Gen2 is a proposed IceCube expansion to 100-300 km<sup>2</sup> scale for the detection of neutrinos above  $10^{13.5}$  eV, focusing on energies above which the atmospheric neutrino background is not overwhelmingly dominant, and with the discovery potential for BZ neutrinos.<sup>20</sup> However, to achieve sensitivity to the full range of BZ neutrino models, we must instead turn to a different detection mechanism that allows us to instrument larger volumes for comparable cost. Neutrino telescopes that utilize the radio detection technique search for the coherent, impulsive radio signals that are emitted by electromagnetic particle cascades induced by neutrinos interacting with a dielectric. Radio UHE neutrino detection requires a volume  $\mathcal{O}(100)$  km<sup>3</sup> of dielectric material, which limits the detection medium to be naturally-occurring, that allows radio signals to pass through without significant attenuation over lengths  $\mathcal{O}(1)$  km. Current and proposed experimental efforts in this field monitor or plan to monitor immense volumes of glacial ice, whose radio attenuation properties have been directly measured at multiple locations in Antarctica and Greenland, and have the desired clarity.<sup>21–26</sup> We note that although IceCube-Gen2 is nominally on an expansion of the array of optical sensors, a radio array component may be considered for enhancement of sensitivity in the energy range  $10^{16}$ - $10^{20}$  eV.<sup>20</sup>

Even some of the most pessimistic models predicting BZ neutrino fluxes are within reach of planned experiments using the radio technique. These more pessimistic models tend to have heavy cosmic-ray composition or a weak dependence of source densities on redshift, within constraints set by other measurements. Recent measurements with the Auger and the Telescope Array disfavor a significant iron fraction in the cosmic-ray composition at energies up to and even exceeding  $10^{19.5}$  eV, which in turn favors higher fluxes of BZ neutrinos than if the highest energy cosmic rays were pure iron.<sup>27,28</sup> An experiment that has a factor of  $\sim 50$  improvement over the best sensitivity currently achieved by IceCube near  $10^{18} - 10^{19}$  eV, or reduces the energy threshold with an ANITA-level sensitivity by about a factor of  $\sim 50$  would reach these pessimistic neutrino flux expectations. For most models, such an experiment would observe enough events to make an important impact in our understanding of UHE astrophysics and particle physics utilizing the highest energy observable particles in the universe. We note, however, that even these pessimistic models can be evaded through alternate explanations for the cosmic ray data, or more exotic scenarios.<sup>7,29,30</sup>

## 2. Motivation for the Radio Technique

### 2.1. Askaryan Effect

In 1962, physicist Gurgen Askaryan predicted that an energetic electromagnetic cascade in a dense dielectric medium should produce observable, coherent electromagnetic radiation.<sup>31</sup> When an energetic charged particle or photon produces an electromagnetic cascade in a dielectric medium, the shower will acquire a  $\sim 20\%$  negative charge excess. This comes about primarily through Compton scattering of electrons in the medium, but also from the annihilation of positrons in the shower with electrons in the medium. If the charge excess is moving at a velocity greater than the phase velocity of light in the medium, the medium will emit Cherenkov radiation. The radiation is emitted most strongly at the angle given by  $\cos \theta = 1/n$  with respect to the shower axis, and the power radiated at optical wavelengths is proportional to the shower energy. In ice, a common medium for detection of neutrino interactions,  $n = 1.78$  at radio frequencies, giving  $\theta = 57^\circ$ . For wavelengths longer than the size of the shower along the transverse dimension (perpendicular to the shower axis), the signal is emitted coherently and the electric field strength is proportional to the shower energy. The Cherenkov radiation is coherent at wavelengths longer than the Molière radius in a dense medium ( $\sim 10$  cm), corresponding to frequencies  $\lesssim 1$  GHz.

The Askaryan effect was first observed in a beam test at SLAC National Accelerator Laboratory in 2001.<sup>32</sup> Using a target of silica sand to produce showers induced by brehmsstrahlung photons from a 28.5 GeV electron beam and a series of broadband, microwave horn antennas with bandwidths covering the range 0.3 to 6 GHz, the beam test showed the first experimental evidence of the coherence effect predicted by Askaryan in the 1960's. The results of the beam test are shown in Figure 2.<sup>32</sup> Figure 2a shows the measured shower profile as a function of distance along the shower axis, with an inset of the time-domain electric field measured near shower maximum. The measured shower profile (diamonds) matches the prediction well, and the signal is broadband and impulsive. Figure 2b shows the measured electric field strength as a function of shower energy, controlled by changing the number of photons that initiated the shower. The linear dependence of the electric field on the energy of the shower is evidence for coherence. Figure 2c shows the measured electric field strength as a function of frequency compared to results from a Monte Carlo simulation.

The observation of the Askaryan effect was confirmed later in rock salt and again in ice at separate subsequent beam tests at SLAC in 2004 and 2006, respectively.<sup>33,34</sup> The observation of the Askaryan effect in ice is of particular note, since many experimental efforts monitor large volumes of naturally occurring ice. Although the lunar regolith (sand) continues to be used as a target for neutrino searches<sup>35,36</sup> and rock salt has been investigated as a potential target medium,<sup>37</sup> most efforts use ice as a target due to its remarkable naturally-occurring volume, radio clarity, and



uniformity.

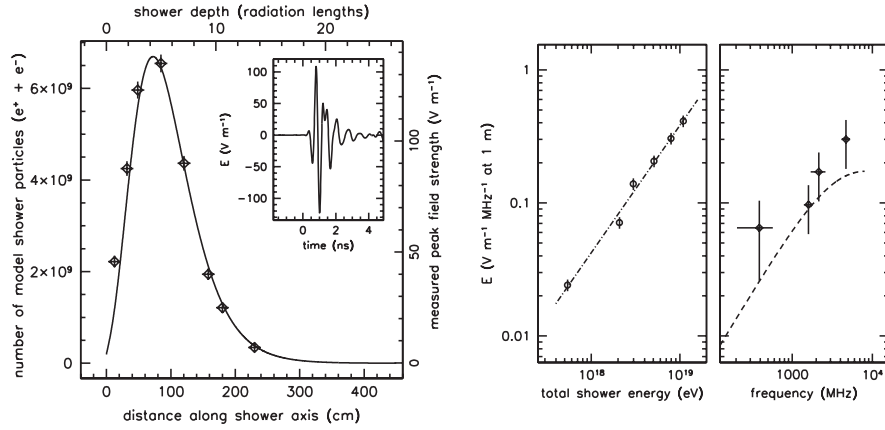


Fig. 2.: The first observation of the Askaryan effect, from Reference.<sup>32</sup> (a) The field strengths closely follow the expected shower profile along the shower axis. The time-dependent electric field measured near shower maximum is shown in the inset. (b) The measured electric field plotted against shower energy. The dashed line shows a least-squares fit to the data, consistent with complete coherence. (c) The measured electric field spectrum compared to a semi-empirical parametrization is shown as a dashed line.

## 2.2. A Radio Clear Dielectric for a Detector

To determine the suitability of different naturally-occurring dielectric media for the detection of radio emission from highly energetic neutrinos, many measurements have been made of the dielectric attenuation at radio frequencies at different sites around the world. The field attenuation length  $L_\alpha$  is defined to be the distance over which the distance-corrected electric field ( $E(r)$ ) drops by a factor of  $1 - 1/e$ . At a distance  $r$ :

$$rE(r) = E(0)e^{-r/L_\alpha}. \quad (1)$$

The following equation given in<sup>26</sup> is useful for relating the field attenuation length reported in particle astrophysics to the dielectric loss per distance  $N_L$  reported by geophysicists:

$$N_L[\text{dB/km}] = 8686.0 \langle L_\alpha[\text{m}] \rangle. \quad (2)$$

Askaryan himself proposed dense media such as ice, salt, and even the lunar regolith for the detection of cosmic ray showers.<sup>31</sup> Ice was later proposed as a promising, cost-effective medium for the detection of showers produced by high energy neutrino interactions as well.<sup>38</sup> Several measurements have confirmed that there are naturally-occurring ice sheets that exhibit the dielectric properties necessary to make an excellent medium for neutrino detection. Measurements in naturally-occurring rock salt have found more modest attenuation lengths, and the lunar regolith has also been used as a target of observation for neutrino interactions above  $\sim 10^{21}$  eV.

### 2.2.1. Attenuation Length of Glacial Ice

One of the most promising sites for a large radio detector is in the ice near the South Pole, which sits atop  $\sim 2.8$  km of radio-clear glacial ice. The measurement of the radio attenuation length in ice at the South Pole with the smallest uncertainties and largest horizontal component<sup>23,24</sup> gives a depth-averaged field attenuation length  $\langle L_\alpha \rangle$  at 300 MHz of  $1600^{+255}_{-120}$  m over the top 1500 m of ice,<sup>24</sup> the depth over which a surface or sub-surface experiment would be the most sensitive to neutrino interactions. This result is derived from a comparison between the amplitude of a broadband signal transmitted from an antenna deployed on an IceCube string 2500 m below the surface and the amplitude of the same signal received at an antenna buried at about 30 m below the surface, 2000 m away horizontally.

A site with similar properties is found at the peak of the high plateau in Greenland, at Summit Station, which sits on top of 3 km of glacial ice. The attenuation length of the ice at Summit Station was measured by bouncing an impulsive radio signal off of the bottom of the glacier, measured at  $3014^{+48}_{-50}$  m depth, and comparing the strength of the return signal to a direct measurement between the transmitter and the receiver through air. The field attenuation length has been measured to be  $\langle L_\alpha \rangle = 947^{+92}_{-85}$  m at 75 MHz averaged over all depths.<sup>25</sup> The power reflection coefficient  $R$  is assumed to be 0.3 for the ice-bedrock interface. For a reasonable extrapolation to higher frequencies, this measurement is consistent with measurements in Reference<sup>39</sup> reported at 150-195 MHz. Accounting for a depth-dependent temperature profile and extrapolating using a frequency dependence of  $-0.55$  m/MHz, based on an ensemble of previous measurements, yields a field attenuation length of  $\langle L_\alpha \rangle = 1022^{+230}_{-253}$  m over the top 1500 m of ice at 300 MHz.<sup>25</sup>

Another promising site is Moore's Bay on the Ross Ice Shelf, where the average measured depth of the ice is  $576 \pm 8$  m.<sup>26</sup> Using a technique where reflection loss (found to be  $-1.7$  dB) is separated from attenuation loss by separating the transmitter and receiver by over 500 m at the surface, the measured depth-averaged field attenuation length  $\langle L_\alpha \rangle$  between 100 and 850 MHz is  $(460 \pm 20) - (180 \pm 40) \nu$  m, where  $\nu$  is the frequency of interest in GHz. This corresponds to a frequency dependence of  $-0.18$  m/MHz.<sup>21,26</sup> The shorter attenuation length at Moore's Bay compared to potential deep sites is due primarily to the fact that the ice is warmer

at Moore's Bay.

### 2.2.2. Attenuation Length of Rock Salt

Large, naturally-occurring deposits of rock salt have also been investigated as a possible detection medium for radio emission from neutrino interactions. Investigations at three different locations in the United States (WIPP in New Mexico, Hockley in Texas, and the Cote Blanche mine operated by the North American Salt Company in St. Mary Parish, Louisiana)<sup>40,41</sup> indicate that the attenuation length of rock salt is heavily dependent on the moisture content, layering, and composition of the salt. The longest attenuation length was measured directly at Cote Blanche by transmitting impulsive, broadband radio signals directly through the salt from a transmitter to a receiver with bandwidths spanning 125 to 900 MHz in boreholes drilled up to 200 ft. into the salt.

The field attenuation length  $\langle L_\alpha \rangle$  at 300 MHz was measured to be  $63 \pm 3$  m at Cote Blanche, which is significantly shorter than measurements of glacial ice have shown. However, the relatively high density of rock salt compared to ice boosts the neutrino interaction cross section by a factor of about 2.5, which would make up for some of the volumetric loss due to the shorter radio attenuation length. In addition, in salt the Cherenkov emission would be broader in solid angle,<sup>42</sup> leading to an increase in achievable effective volume, and an overburden of bedrock would block backgrounds from above such as galactic noise and cosmic rays.

### 2.2.3. Attenuation Length of Lunar Regolith

The lunar regolith is another possible radio-transparent target for interactions of highly energetic neutrinos. The radio attenuation length of samples that have been returned to Earth has been shown to be  $\mathcal{O}(20)$  m at 1 GHz and  $\mathcal{O}(200)$  m at 100 MHz,<sup>43</sup> comparable to that of rock salt. However, these values were found to vary across samples, depending on their exact composition. Although estimates of the depth of the moon's regolith vary widely, and is expected to vary over the lunar surface, conservative depth estimates are near 10 m.<sup>44</sup> Sensitivity estimates for the Goldstone Lunar Ultra-high-energy Neutrino Experiment (GLUE) experiment assume a 10 m regolith depth, while estimates for the NuMoon experiment assume a depth of up to 500 m.<sup>45,46</sup>

## 3. Experimental Strategies

### 3.1. Assessing the Sensitivity of an Experiment

There are a few factors that determine the number of neutrinos expected to be detected from a given experiment, and these are the factors that go into an experimental design. We often define an energy-dependent, water-equivalent effective volume $\times$ solid angle  $[V\Omega]_{\text{eff}}(E)$  for an experiment, where  $E$  is the neutrino energy,

and it is given by

$$[V\Omega]_{\text{eff}}(E) = V \cdot 4\pi \cdot \varepsilon_V(E) \cdot \rho_{\text{H2O}}/\rho_{\text{det}}, \quad (3)$$

where  $V$  is the total volume of the detection medium,  $\varepsilon_V(E)$  is the fraction of neutrinos interacting in that volume that pass the trigger, and  $\rho_{\text{det}}/\rho_{\text{H2O}}$  is the density of the detection medium relative to water. In order to predict the number of neutrino events  $N$  detected in an experiment from a given flux model  $F(E) = dN/dE/d\Omega/dt$ , we need to define an effective area×solid angle  $[A\Omega]_{\text{eff}}(E)$  so that

$$N = \int F(E) \cdot [A\Omega]_{\text{eff}}(E) \cdot T \cdot dE, \quad (4)$$

where  $T$  is the livetime of the experiment. If the thin-target approximation is valid, i.e., the dimensions of the detection medium are much smaller than the interaction length  $\ell(E)$ , then we can take  $[A\Omega]_{\text{eff}}(E) = [V\Omega]_{\text{eff}}(E)/\ell(E)$ .

The effective area typically increases with energy, and there is some energy below which the experiment does not expect to see a significant number of events. This is called the energy threshold, and is not well-defined quantitatively, but is set by the energy-dependent efficiencies at the trigger and analysis stages (analysis efficiencies are not included in the above equations). In turn, the trigger efficiencies are set by the trigger thresholds necessary to maintain the rate of data acquisition that is possible given the level of thermal noise that is seen. Since the high-energy neutrino flux (from GZK models and direct production models) is a falling spectrum at high energies, the event rate can be strongly dependent on the energy threshold.

### 3.2. Experimental Approaches

Although most experiments that aim to detect radio emission from high energy neutrino interactions are similar in their approach, determining the best experimental configuration is a tradeoff among a variety of factors. All experiments that rely on observations of Askaryan emission need to monitor a large volume of radio-transparent dielectric. However, many different approaches have been explored, such as the observation of the Antarctic continent or Greenland from a balloon or satellite, ground-based techniques that deploy instruments directly on the surface or at depth surrounded by large volumes of ice or salt, and observation of the lunar regolith from afar. Other experiments seek the radio emission produced by an air shower resulting from the decay products of a tau lepton produced from a neutrino interaction. All have different benefits and drawbacks.

#### 3.2.1. Experiments Using the Askaryan Technique

We can see the trade-off between balloon-borne experiments and detectors on the ground in terms of the variables defined in Section 3.1. Putting a detector farther from the neutrino interactions increases the energy threshold. However, from high altitudes an experiment can view a larger area of ice compared to an experiment on

the ground, which increases  $[A\Omega]_{\text{eff}}$ . In general, detectors that observe large volumes from far distances (from a balloon, satellite, or viewing the moon) are the best probes of the flux of the highest energy neutrinos. We will call these “view-from-a-distance” experiments. Balloon experiments such as ANITA<sup>47</sup> and the proposed ExaVolt Antenna (EVA)<sup>48</sup> fly at  $\sim 37$  km altitude above the Antarctic ice sheet. ANITA has set the strongest limits above  $10^{19.5}$  eV. Telescopes such as the Parkes Lunar Radio Cherenkov Experiment<sup>49</sup> aimed at the moon are seeking Askaryan emission from the sandy regolith at the lunar surface. The PRIDE experiment is even exploring other worlds as possible detection media, such as Enceladus or Europa, icy moons of Saturn and Jupiter, respectively.<sup>50</sup>

Detectors on the ground or embedded in their detection medium, such as the Askaryan Radio Array (ARA) and The Antarctic Ross Ice Shelf Antenna Neutrino Array (ARIANNA), which sit in and on glacial ice, have a lower energy threshold than ones that are situated farther from the interactions. In addition, the livetime can be much longer for an embedded experiment compared to a balloon experiment (years compared to several weeks). The drawback of being so close to the interactions is that a smaller volume of ice can be monitored by each detector element compared to from above, which reduces  $[A\Omega]_{\text{eff}}$  for the same number of detectors. Therefore, embedded detectors consist of an array of antennas covering a large area.

View-from-a-distance experiments and in-ice experiments utilizing the Askaryan technique thus have different strengths for probing high energy astrophysics. For example, experiments that view from far distances have the greatest potential to measure the high energy cutoff of the astrophysical sources. Experiments on the ground, due to their lower threshold, are necessary to reach the heart of the GZK-induced neutrino spectrum, predicted to be at about  $10^{18}$  eV, and if thresholds can be reduced, could measure the astrophysical neutrino spectrum above the  $\sim 1$  PeV energies corresponding to the highest energy events so far observed by IceCube.

Once neutrino events are observed, embedded detectors also have the potential to achieve better angular resolution for neutrinos. By placing detectors relatively far apart (tens of meters), one can in principle view the Cherenkov cone from different angles, and use measured polarizations to reconstruct the direction of the shower and thus the neutrino direction. This is unlike a balloon-borne experiment whose size is tightly constrained. The energy resolution is also improved with the ability to pinpoint the neutrino interaction location. Although these techniques are not yet mature, their development will become of extreme importance as soon as the first neutrinos are measured using the radio technique.

A few experiments pioneered the radio technique to search for high energy neutrinos by searching for the Askaryan signature in various media. Data from the FORTE<sup>51</sup> satellite was used to search for neutrino interactions in Greenland ice in the late 1990's. The Parkes Lunar Radio Cherenkov Experiment, followed by the GLUE experiment at the Goldstone Observatory in California, both searched for neutrino interactions in the moon's regolith.<sup>45,49,52</sup> RICE was an array of radio

antennas that was deployed on strings of AMANDA (the predecessor of IceCube), ran from 1999-2011, and published competitive limits as can be seen in Figure 1.<sup>14</sup>

### 3.2.2. *Experiments Using the Air Shower Technique*

There are also experimental efforts to demonstrate techniques required to detect radio emission from extended air showers induced by neutrino interactions. Tau neutrinos that undergo a charged current interaction in the Earth and are moving at a slight up-going angle or interact in a mountain produce a tau lepton that emerges from the Earth's surface and decays in the atmosphere. The charged particles in the shower(s) resulting from the tau decay generate radio emission in part due to a geomagnetic effect: positively and negatively charged particles are split due to the Earth's magnetic field, yielding geosynchrotron emission. Askaryan radiation is also emitted from the shower. Detection of radio emission from cosmic-ray air showers has been made by a variety of experiments,<sup>53-56</sup> but neutrino-induced air showers are much more rare and have yet to be detected. Auger looks for air showers induced by decays from tau leptons that might emerge from neutrino interactions in the Andes Mountains.<sup>13</sup> The TREND project was designed as a prototype to demonstrate the technique,<sup>55,57</sup> and recently the Giant Radio Array for Neutrino Detection (GRAND) experiment has been proposed to detect radio emission from neutrino-induced extended air showers.<sup>58</sup>

## 4. Balloon Experiments

### 4.1. *ANITA: The Antarctic Impulsive Transient Antenna*

The ANITA experiment flies under NASA's Long-Duration Balloon program, lifted to 37 km altitude over the Antarctic continent by a balloon that is  $\sim 100$  m in diameter at altitude. ANITA searches for radio signals from neutrinos interacting in the ice sheet below. With the horizon at  $\sim 700$  km distance at float altitude, ANITA uses all of its visible Antarctic ice sheet as its neutrino detection volume. The instrument can view  $\sim 1.5 \times 10^6$  km<sup>2</sup> of ice at altitude, and is designed to search for impulsive, broadband signals predominantly in the vertical polarization emerging from the ice below the payload. ANITA uses dual-polarization (horizontal and vertical), quad-ridged horn antennas with 200-1200 MHz bandwidth. For each channel (one polarization of one antenna), the signal at the antenna output is amplified and filtered before being split so that it can be sent through both the trigger and readout chains. Each channel is Nyquist-sampled and read out with fast ( $> 2$  GSa/sec) digitization, producing a  $\sim 100$  ns waveform for each channel when a multi-level trigger is satisfied. ANITA-1 was launched in December 2006 and was aloft for 35 days, ANITA-2 flew in 2008-09 for 31 days, and ANITA-3 flew in 2014 for 22 days.

There are two main types of triggered events that need to be rejected in order to

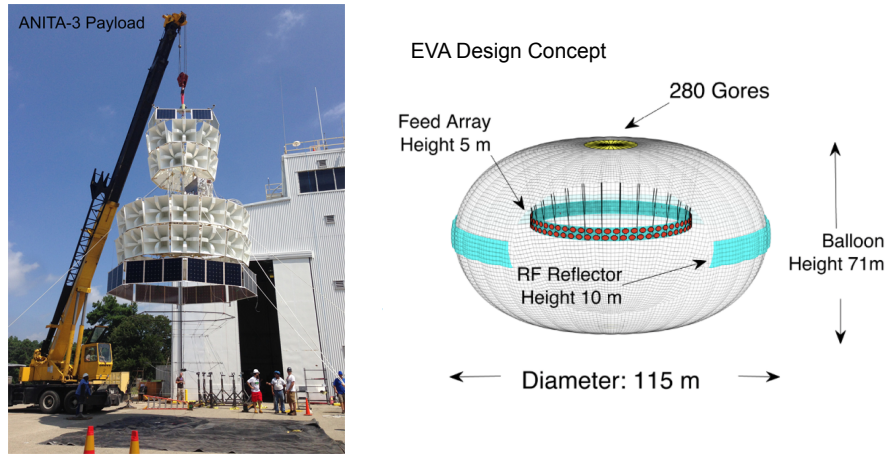


Fig. 3.: Left: A picture of the ANITA-3 payload, fully integrated in August 2014 in preparation for its Antarctic flight in December 2014. ANITA-3 has 96 channels, as well as a low-frequency antenna for cosmic-ray science (visible below the payload in the picture) that was dropped down below the payload after launch. Right: a sketch of the EVA concept, credit to Peter Gorham.

search for neutrino candidate events: thermal noise events and human-made noise events. Thermal noise backgrounds are reduced by requiring a high signal-to-noise ratio, a high cross-correlation between waveforms with time delays expected from an incoming plane wave, and a linearly polarized signal. Events that contain modulated, continuous-wave (CW) signals are subject to a notch-filter, which removes power in a narrow band surrounding any peaks in the measured spectrum above a threshold.

ANITA has published results from searches for a diffuse neutrino flux in each of its first two flights, and also reported a targeted search for neutrinos from Gamma Ray Bursts (GRBs) using data from its second flight. ANITA searches for isolated signals from the ice that are not associated with any known bases or with any locations with repeating signals. A blind analysis of data from the second flight of ANITA rejected thermal noise by a factor of  $\leq 2.5 \times 10^{-8}$  and yielded one candidate neutrino event on an expected background of  $0.97 \pm 0.42$  events. This search produced what is still the world's best limit on the neutrino flux at energies greater than  $10^{19.5}$  eV.<sup>15,16</sup> A set of baseline models for cosmogenic neutrino fluxes would predict 0.3-1.0 neutrinos to pass the cuts. A targeted search for neutrinos associated with GRBs was done by narrowing the time window of interest to the 10 minutes surrounding 12 known GRBs that occurred during the second flight of ANITA when the payload was located in quiet regions of Antarctica. The strategy of conducting the search over a reduced time period leads to reduced backgrounds compared to the diffuse search, allowing for the analysis cuts to be loosened. The two hours of data surrounding each GRB, excluding the 10 minute window of interest, was used

to estimate the background and set the cuts. The GRB search yielded no candidate events and the best limit on the fluence of neutrinos associated with GRBs at extremely high energies.<sup>59</sup>

ANITA-1 also reported the observation of 16 cosmic rays from geosynchrotron emission. For 14 of the events, the impulses were observed after a reflection from the ice surface, and were flipped in polarity compared to the remaining two events that were observed directly.<sup>53</sup>

ANITA-3 flew 48 antennas compared to 40 in ANITA-2, and triggered on both polarizations (cosmic ray air showers are detected in the horizontal polarization<sup>53</sup>), with a noise-riding trigger threshold. These improvements led to a factor of  $\sim 5$  improvement in expected neutrino event rates compared to ANITA-2. ANITA-3 also included a low-frequency omnidirectional antenna (ALFA), providing additional information for the hundreds of UHE cosmic-ray events that are expected to have been recorded by ANITA-3 via radio emission from cosmic-ray induced atmospheric extended air showers. The left-hand panel of Figure 3 is a picture of the ANITA-3 payload, fully integrated in August 2014 in advance its December 2014 flight.

#### **4.2. EVA: The ExaVolt Antenna**

Building on ANITA's strategy of utilizing NASA's long-duration balloons to carry out searches for neutrinos in the UHE regime, EVA<sup>48</sup> is an ambitious project aiming to transform a 100 m-scale balloon into a high gain, toroidal reflector antenna (see the right-hand panel of Figure 3). The increase in gain compared to ANITA would mean a  $\gtrsim 100$  times reduction in threshold in power, and thus a  $\gtrsim 10$  times reduction in threshold in field strength and neutrino energy. What makes the EVA concept feasible is the super-pressure balloon (SPB) technology currently under development by NASA,<sup>60</sup> where the inside of the balloon is kept at a higher pressure than the outside ambient pressure, with differential pressures up to 180 Pa, keeping the shape of the balloon nearly unchanged over a flight. A test flight in 2008 over Antarctica, SPB flight 591NT, reported that the height and diameter of a 7 Mft<sup>3</sup> balloon changed by 1% in a 54 day flight.<sup>61</sup>

In September of 2014, the EVA team carried out a test of a prototype instrumented SPB in a hangar at NASA's Wallops Test Facility to demonstrate that a feed array could be deployed inside of a SPB, and that the balloon could be instrumented with an RF reflector-receiver system that could be well understood by modeling.<sup>62</sup> The 1:20 scale prototype was a 5.7 m SPB balloon. Reflector tape was attached to the balloon near its equator and a feed array membrane held the receivers (dual-polarized sinuous patch antennas) and associated electronics over a section of its circumference for the test (see Figure 4).

An impulsive plane-wave calibration signal was sent to the balloon and was observed at incidence and after reflection. A comparison of the two pulses is consistent with detailed time-domain modeling of the prototype, and the team is currently preparing to propose a flight of a full EVA.



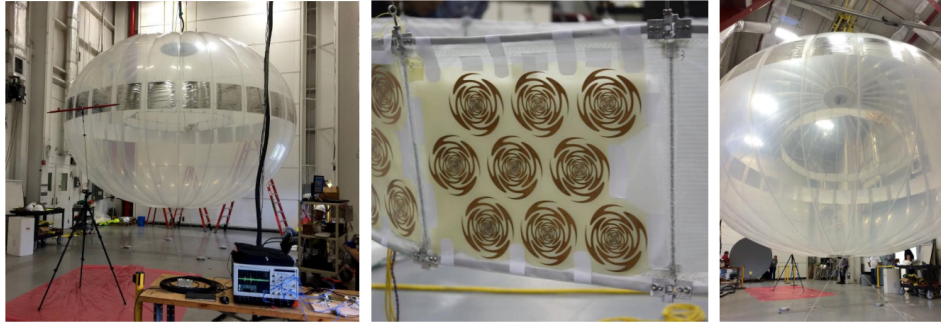


Fig. 4.: Pictures of the EVA prototype test (balloon, toroidal reflector, and dual-polarized sinuous feed antennas) at NASA's Wallops Test Facility.<sup>62</sup> Photo credit to Peter Gorham.

## 5. Ground-Based Experiments

### 5.1. Askaryan Effect in Ice

#### 5.1.1. ARA: The Askaryan Radio Array

The Askaryan Radio Array (ARA) is a radio array embedded in the ice near the South Pole with the aim of measuring cosmic neutrinos in the energy regime above  $\sim 10^{17}$  eV. Searching for Askaryan emission from neutrino interactions in the deep ice near the South Pole, stations of receiver antennas are deployed in dry holes at 200 m depth. A schematic of the ARA design is shown in Figure 5. Each station consists of 16 antennas, each of which is read out as a separate channel. Each ARA station uses a mixture of antennas designed to measure vertical and horizontal polarizations, deployed along four strings separated by  $\sim 10$  m. Calibration pulsers and associated transmitting antennas are also deployed with each station along additional strings.

The trigger and readout chains are similar to ANITA, but the digitized waveforms are  $\sim 250$  ns in length. The trigger currently requires that some number of channels in a station (typically 3 out of 16) exceed a power threshold ( $\sim 5-6$  times the mean power) within a 110 ns time window, approximately the time it takes a signal to traverse a station.

An initial Testbed prototype station was deployed in the 2010-2011 season at  $\sim 30$  m depth, followed by the first full station (A1) in 2011-2012 at 100 m depth. Two other stations, A2 and A3, have been in the ice at 200 m depth since the 2012-2013 season. All three deep stations are currently operational. Two more stations, A4 and A5, will be deployed in the 2017-2018 season.

ARA neutrino searches look for signals that could have originated from neutrino interactions in the ice and reject events that reconstruct to the South Pole Station.

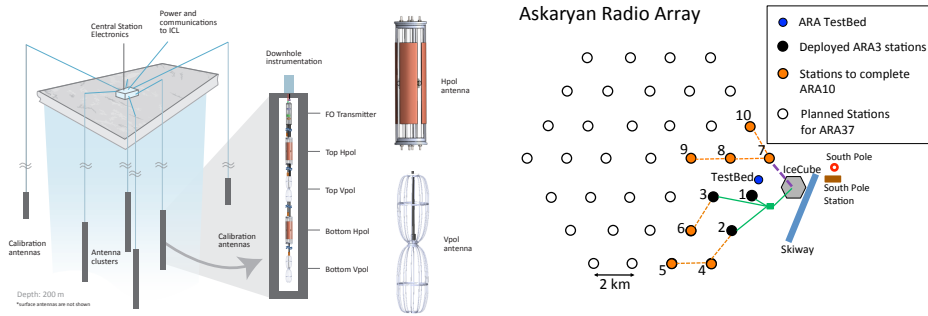


Fig. 5.: Left: the baseline design of an ARA station showing the details of one string and a drawing of the antennas sensitive to each linear polarization, from Reference.<sup>63</sup> Right: a map of the proposed locations of ARA stations at the South Pole, from Reference.<sup>64</sup> Currently there are three stations deployed (shown in black), plus a testbed (in blue).

Interferometric techniques, with timing based on cross-correlations between waveforms from different antennas, are used to reconstruct directions of signals. ARA has the capability to take into account the bending of the trajectories of signals in the firm near the surface, where the index of refraction changes with depth. Thermal noise is reduced through requirements that the timing of the signals in the antennas is consistent with a real signal crossing the detector.

Using the ARA Testbed station, ARA carried out a search for cosmic neutrinos from diffuse sources, and then a targeted search for neutrinos from GRBs, with 415 days of livetime using the 2011-2012 data from the ARA Testbed.<sup>64,65</sup> As was done for the ANITA GRB search, neutrinos were sought in a 10 minute time window surrounding the occurrence of each of 57 GRBs. This resulted in the first quasi-diffuse limit on the GRB flux above  $10^{16}$  eV. The quasi-diffuse limit is based on the assumption that the 57 GRBs considered for the analysis were representative of all GRBs.

ARA has completed a first search for neutrinos from two of the three deployed deep stations (A2 and A3) using 10 months of data from 2013.<sup>63</sup> No candidates were observed on a background of  $0.009 \pm 0.010$  for A2 and  $0.011 \pm 0.015$  for A3, resulting in constraints on the cosmic neutrino flux.

### 5.1.2. ARIANNA: The Antarctic Ross Ice Shelf Antenna Neutrino Array

ARIANNA is a proposed ground-based array of radio antennas on the Ross Ice Shelf in Antarctica.<sup>66</sup> An ARIANNA array of  $\sim 1000$  autonomously-powered detectors would achieve a sensitivity similar to a 37-station ARA array. Although a 1000-station wind-powered ARIANNA design has been considered, a 1296 ( $36 \times 36$ ) station array can be powered via solar power and battery backup for the same cost.

ARIANNA's shallow design with no drilling needed makes an ARIANNA station simpler to deploy than an ARA station. ARIANNA's proposed  $36 \times 36$  station array would span more than  $1000 \text{ km}^2$  on the  $\sim 600 \text{ m}$ -deep Ross Ice Shelf compared to an ARA37 that would span  $\sim 100 \text{ km}^2$  area at the South Pole where the ice is  $\sim 2800 \text{ m}$  deep. There is a reflecting layer of ocean water at the bottom of the Ross Ice Shelf that acts as a mirror, reflecting radio signals from down-going neutrinos back up to the antennas on the surface of the snow.<sup>67</sup> This means that ARIANNA would have a broader range in visible solid angle compared to ARA due to the ability to see down-going neutrinos, which counteracts the shorter measured radio attenuation length of the ice on the Ross Ice Shelf.

An ARIANNA station, shown in Figure 6, consists of high-gain log-periodic dipole antennas (LPDAs) with a bandwidth of  $\sim 0.08\text{--}1.3 \text{ GHz}$  in snow that are downward-pointing and deployed near the surface of the snow. The HRA (Hexagonal Radio Array) consists of eight prototype stations, most consisting of four LPDAs, and was deployed in the Austral summers of 2012-2013 and 2014-2015. A design station for the full ARIANNA array would contain 6-8 downward-facing LPDAs. When a multi-level trigger is satisfied at a station, waveforms across that station are digitized at  $2 \text{ GSa/sec}$ . Stations are solar powered, with battery backups that both provide power on cloudy days and extend the life of the stations a few weeks past sundown in low power mode, as discussed in Reference.<sup>68</sup> The achieved livetime is 58% of the year.<sup>69</sup>

ARIANNA performed a first neutrino search using data from the HRA. After searching for events that contain impulsive signals whose arrival times are consistent with a plane wave crossing the station in the absence of any narrow peak in the Fourier spectrum pointing to CW noise, no neutrino candidates were found in four months of operation. From those results, ARIANNA set its first limit on the diffuse



Fig. 6.: View of one ARIANNA station with solar panels on a tower. The box containing the station's data acquisition box is buried in the ice beneath the tower. Photo credit to Chris Persichilli.

neutrino flux above  $10^{17}$  eV with three HRA stations.<sup>70</sup> Data from all eight stations of the HRA is currently being analyzed.

### 5.1.3. *GNO: The Greenland Neutrino Observatory*

An effort is ongoing to develop Summit Station, a year-round station run by the National Science Foundation (NSF), as a site for radio detection of UHE neutrinos. The ice at Summit Station is comparable to that at the South Pole in radio clarity (see Section 2.2.1) and in thickness (3000 m at Summit Station compared to 2800 m at South Pole), but with a shallower firn allowing for shallower deployment of sub-surface antennas. At Summit Station, at 100 m depth the firn density has reached 95% that of deep ice, compared to 140 m at the South Pole.<sup>71,72</sup> A first prototype station for GNO was deployed in the Summer of 2015 to monitor the radio-frequency noise environment.

## 5.2. *Lunar Experiments*

In 1995, the Parkes Lunar Radio Cherenkov Experiment, using the 64 m Parkes radio telescope, was the first to search for radio emission from neutrino interactions in the moon's regolith, the loose,  $\sim 10$  m deep layer at the surface of the moon. Due to the expected geometry of neutrino-induced events, lunar radio experiments are expected to be sensitive to neutrinos when viewing the lunar "limb" (the edge of the moon's visible surface).<sup>73</sup> Multiple antennas are beamed for heightened sensitivity to regions along the limb. Radio frequency interference is often reduced in lunar radio experiments by requiring signals in different frequency bands to arrive at the delays expected from dispersion through the ionosphere. GLUE was the next to search for highly energetic neutrino interactions in the moon's regolith in 2000-2003 using the 34 m DSS13 and 70 m DSS14 antennas at the Goldstone Observatory in California for 124 h of observing time, constraining the neutrino flux at energies above  $10^{21}$  eV.<sup>45,49</sup> Since then, a series of experiments have followed up with lunar observations with radio telescopes.<sup>52,74-79</sup> The NuMoon experiment observed the moon with the Westerbork Synthesis Radio Telescope array in four frequency bands between 113 and 175 MHz for 47.6 hours, and claims the most competitive constraints on the neutrino flux above  $10^{23}$  eV, as seen in Figure 1.<sup>18</sup> Lunar observations have been proposed with the Low Frequency Array (LOFAR), a recently completed radio antenna array with beaming accomplished electronically rather than mechanically, with a sensitivity projected to improve upon the NuMoon constraints by a factor of 25 as stated in Reference.<sup>18</sup> The Square Kilometer Array (SKA) will be even more sensitive to neutrinos from the moon with this technique due to its wide bandwidth and large collecting area. Construction of Phase 1 of SKA is scheduled to begin in 2018.<sup>80</sup>

### 5.3. Neutrino-Induced Air Showers

Auger searches for neutrinos in the UHE regime by distinguishing “young” and “old” showers using their 1600 Surface Detectors, each consisting of a Cherenkov tank with photomultipliers read out with flash analog to digital converters (FADC) with 25 ns resolution.<sup>13</sup> Protons, heavy nuclei and any gamma rays are expected to shower soon after they hit the atmosphere, so by the time their showers hit Auger’s Surface Detectors they are old showers, consisting mainly of muons with highly coincident arrival times. Neutrinos however, are equally likely to interact anywhere along their path through the atmosphere, and therefore can be young when they arrive at the Surface Detectors. Also, a tau neutrino can interact and produce a tau lepton in mountains surrounding the observatory and the subsequent tau decay would lead to a young shower seen by Auger. Younger showers would still contain an electromagnetic component when they are observed and would show a broader distribution of arrival times. The greatest separation between young and old showers is expected for events that are highly inclined. Auger sets competitive limits on the tau neutrino diffuse flux only, to which they are the most sensitive. Auger’s competitive UHE neutrino flux limit shown in Figure 1 is a tau neutrino limit multiplied (i.e. weakened) by a factor of 3 for comparison with other experiments whose limits are averaged over all flavors.

The proposed GRAND experiment would consist of an array of antennas in a remote mountainous site to search for air showers induced by the decay of tau leptons in the atmosphere that originate from a charged current interaction of tau neutrinos with the Earth.<sup>58</sup> The GRAND collaboration proposes the deployment of  $\mathcal{O}(10^5)$  radio antennas, operating between 30–100 MHz and covering  $\mathcal{O}(10^5)$  km<sup>2</sup> at a site in the Tianshan mountains in China. The preliminary design includes several sub-arrays, each with area  $\mathcal{O}(10^4)$  km<sup>2</sup>. Initial estimates predict that a  $6 \times 10^4$  km<sup>2</sup> array would have an effective area several times larger than ARA’s effective area between  $10^{18}$ – $10^{19}$  eV, and a  $2 \times 10^5$  km<sup>2</sup> array would further improve the sensitivity by a factor of  $\sim 10$  in the same energy region.

## 6. Goals of Future Experimental Efforts

The most important aim in this field at present is to make a first discovery of neutrinos in the UHE regime. Alongside the firm expectation of the BZ neutrino flux, there is an expected neutrino flux from the astrophysical sources themselves that may be comparable. Once the initial discovery is made, it will open up a unique window to the universe at the highest energies. We will likely be able to say that the highest energy cosmic rays are not purely heavy composition, and that no new physics prohibits a UHE neutrino from reaching us from cosmic distances. We will know the detector effective area that is needed to measure a large enough sample of neutrinos to carry out a particle physics and astrophysics program in this new frontier. In addition, a first discovery will heighten the urgency to develop the

tools to reconstruct neutrino directions and measure neutrino energies, which will be necessary as physics priorities are pursued beyond the implications of the first detection.

Both view-from-a-distance and embedded experiments are working to reduce their energy thresholds, which would move their sensitivities to the *left* in Figure 7, and increase their chance of a discovery with a falling neutrino spectrum. In this figure, one can see the effect of EVA's factor of  $\gtrsim 10$  reduction in energy threshold compared to ANITA. Many experiments are working to implement the interferometric techniques that have been successful at the analysis stage to their trigger stage, to enable detection of lower energy events.<sup>81,82</sup> With an interferometric phased array trigger coherently summing hundreds of antennas, in-ice experiments may be able to lower their thresholds enough to reach the higher end of the PeV neutrino spectrum observed by IceCube<sup>9,10</sup> and ascertain whether the spectrum cuts off or continues to higher energies.<sup>82</sup>

Experiments are also working to increase their effective area in order to move their sensitivities *down* in Figure 7. Ground-based projects ARA and ARIANNA are working to expand their detectors, adding as many stations as funding and logistics allow. The GRAND experiment described in Section 5.3 is looking to utilize a vast swath of the atmosphere to seek neutrino-induced extended air showers and will compete with ARA in the same energy range.

The radio technique for neutrino detection allows experimenters to instrument the immense volumes needed for sensitivity to the rare fluxes of neutrinos expected in the UHE regime through a variety of projects that view the detection medium from within, with embedded detectors such as ARA or ARI-

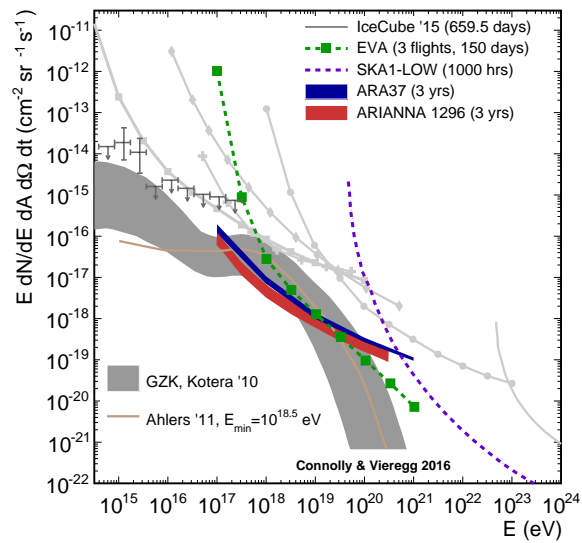


Fig. 7.: The sensitivity reach of future radio neutrino experiments at ultra-high energies and above. We show projected limits for ARA37, EVA and SKA Phase 1 with the low frequency antennas.<sup>62,64,80</sup> In light gray we also show the current most competitive limits that were shown in Figure 1 for comparison.

ANNA, or from a distance, with balloon experiments such as ANITA. Radio telescopes pointed at the moon such as NuMoon are the most sensitive at even higher energies. Other projects, such as Auger, search for UHE neutrinos through an air shower signature. Radio techniques provide an opportunity for a long-term UHE astrophysics program that can reach even some of the most pessimistic predictions for the neutrino flux in the UHE regime. The results from the first decade and a half of neutrino searches in this field and the projections for future experiments portend an exciting future.

## 7. Acknowledgements

The authors would like to thank Tom Gaisser and Albrecht Karle for inviting us to write this contribution. We are also grateful to Jordan Hanson, Clancy James, Andrew Romero-Wolf and David Saltzberg for helpful feedback. A. Connolly would also like to thank the National Science Foundation for their support through CAREER award 1255557, BIGDATA Grant 1250720, Grant 1404266 for ARA support, and NASA for their support through Grant NNX12AC55G for EVA development. A. Connolly would also like to thank the United States-Israel Binational Science Foundation for their support through Grant 2012077. A. Connolly and A. Vieregg would like to thank NASA for their support for ANITA through Grant NNX15AC20G. We are grateful to the U.S. National Science Foundation-Office of Polar Programs. A. Vieregg would like to thank the Kavli Institute for Cosmological Physics for their support, and A. Connolly would like to thank the Ohio State University for their support.

## References

1. K. Greisen, End to the Cosmic-Ray Spectrum?, *Phys. Rev. Lett.* **16**, 748–750, (1966).
2. G. T. Zatsepin and V. A. Kuz'min, Upper Limit of the Spectrum of Cosmic Rays, *JTEP Lett.* **4**, 78, (1966).
3. V. S. Berezinsky and G. T. Zatsepin, Cosmic rays at ultra high energies (neutrino?), *Phys. Lett. B.* **28**, 423–424, (1969).
4. V. S. Berezinsky and G. T. Zatsepin, *Sov. J. Nucl. Phys.* **11**, 111, (1970).
5. A. Connolly, R. S. Thorne, and D. Waters, Calculation of High Energy Neutrino-Nucleon Cross Sections and Uncertainties Using the MSTW Parton Distribution Functions and Implications for Future Experiments, *Phys. Rev. D.* **83**, 113009, (2011).
6. S. R. Klein and A. Connolly, Neutrino Absorption in the Earth, Neutrino Cross-Sections, and New Physics. (2013). arXiv:1304.4891.
7. P. W. Gorham et al., Implications of ultra-high energy neutrino flux constraints for Lorentz-invariance violating cosmogenic neutrinos, *Phys. Rev. D.* 86(10):103006, (2012).
8. L. A. Anchordoqui et al., End of the cosmic neutrino energy spectrum, *Phys. Lett. B.* **739**, 99–101, (2014).
9. M. G. Aartsen et al., First Observation of PeV-Energy Neutrinos with IceCube, *Phys. Rev. Lett.* 111(2):021103, (2013).

10. M. G. Aartsen et al., Observation of High-Energy Astrophysical Neutrinos in Three Years of IceCube Data, *Phys. Rev. Lett.* **113**(10):101101, (2014).
11. M. Ahlers and F. Halzen, Minimal cosmogenic neutrinos, *Phys. Rev. D.* **86**(8):083010, (2012).
12. K. Kotera, D. Allard, and A. V. Olinto, Cosmogenic neutrinos: parameter space and detectability from PeV to ZeV, *J. Cosm. and Astropart. Phys.* **10**:013, (2010).
13. A. Aab et al., Improved limit to the diffuse flux of ultra-high energy neutrinos from the Pierre Auger Observatory, *Phys. Rev. D.* **91**, 092008, (2015).
14. I. Kravchenko et al., Updated results from the RICE experiment and future prospects for ultra-high energy neutrino detection at the South Pole, *Phys. Rev. D.* **85**(6):062004, (2012).
15. P. W. Gorham et al., Observational Constraints on the Ultra-high Energy Cosmic Neutrino Flux from the Second Flight of the ANITA Experiment, *Phys. Rev. D.* **82**(2):022004, (2010).
16. P. W. Gorham et al., Erratum: Observational Constraints on the Ultra-high Energy Cosmic Neutrino Flux from the Second Flight of the ANITA Experiment. (2010). arXiv:1011.5004.
17. M. G. Aartsen et al., The IceCube Neutrino Observatory - Contributions to ICRC 2015 Part II: Atmospheric and Astrophysical Diffuse Neutrino Searches of All Flavors. (2015). arXiv:1510.05223.
18. S. Buitink et al., Constraints on the flux of ultra-high energy neutrinos from Westerbork Synthesis Radio Telescope observations, *Astronomy & Astrophysics.* **521**, A47, (2010).
19. M. Ackermann et al., Optical properties of deep glacial ice at the South Pole, *J. Geophys. Res.* **111**(D13), D13203, (2006).
20. M. G. Aartsen et al., IceCube-Gen2: A Vision for the Future of Neutrino Astronomy in Antarctica. (2014). arXiv:1412.5106.
21. T. Barrella, S. Barwick, and D. Saltzberg, Ross Ice Shelf in situ radio-frequency ice attenuation, *J. Glaciol.* **57**, 61–66, (2011).
22. D. Z. Besson et al., In situ radioglaciological measurements near Taylor Dome, Antarctica and implications for ultra-high energy (UHE) neutrino astronomy, *Astropart. Phys.* **29**, 130–157, (2008).
23. S. Barwick et al., South Polar in situ radio-frequency ice attenuation, *J. Glaciol.* **51**, 231–238, (2005).
24. P. Allison et al., Design and initial performance of the Askaryan Radio Array prototype EeV neutrino detector at the South Pole, *Astropart. Phys.* **35**, 457–477, (2012).
25. J. Avva et al., An in situ measurement of the radio-frequency attenuation in ice at Summit Station, Greenland, *J. Glaciol.* **61**, 1005–1011, (2015).
26. J. Hanson et al., Radar Absorption, Basal Reflection, Thickness, and Polarization Measurements from the Ross Ice Shelf, *J. Glaciol.* **61**, 438–446, (2015).
27. Pierre Auger Collaboration, Depth of Maximum of Air-Shower Profiles at the Pierre Auger Observatory. II. Composition implications, *Phys. Rev. D.* **90**(12):122006, (2014).
28. R. U. Abbasi et al., Study of Ultra-High Energy Cosmic Ray composition using Telescope Array's Middle Drum detector and surface array in hybrid mode, *Astropart. Phys.* **64**, 49–62, (2015).
29. M. Unger, G. R. Farrar, and L. A. Anchordoqui, Origin of the ankle in the ultra-high energy cosmic ray spectrum, and of the extragalactic protons below it, *Phys. Rev. D.* **92**(12), 123001, (2015).
30. N. Globus, D. Allard, and E. Parizot, A complete model of the cosmic ray spectrum and composition across the Galactic to extragalactic transition, *Phys. Rev. D.* **92**(2),



- 021302, (2015).
31. G. Askaryan, Excess Negative Charge of an Electron-Photon Shower and its Coherent Radio Emission, *Soviet Physics JETP-USSR*. **14** (2), 441–443, (1962).
  32. D. Saltzberg and et al., Observation of the Askaryan Effect: Coherent Microwave Cherenkov Emission from Charge Asymmetry in High-Energy Particle Cascades, *Phys. Rev. Lett.* **86**, 2802, (2001).
  33. P. W. Gorham et al., Accelerator measurements of the Askaryan effect in rock salt: A roadmap toward teraton underground neutrino detectors, *Phys. Rev. D*. **72**(2):023002, (2005).
  34. P. W. Gorham et al., Observations of the Askaryan Effect in Ice, *Phys. Rev. Lett.* **99** (17):171101, (2007).
  35. S. Buitink et al. Searching for neutrino radio flashes from the Moon with LOFAR. In eds. R. Lahmann et al., *American Institute of Physics Conference Series*, vol. 1535, pp. 27–31, (2013).
  36. J. D. Bray et al. LUNASKA neutrino search with the Parkes and ATCA telescopes. In eds. R. Lahmann et al., *American Institute of Physics Conference Series*, vol. 1535, pp. 21–26, (2013).
  37. A. Connolly et al., Status of SalSA. (2010). arXiv:1010.4347.
  38. I. M. Zheleznykh. In ed. R. Prothro, *Proceedings of the 21st International Cosmic Ray Conference*, vol. 6, pp. 528–533, (1989).
  39. J. A. MagGregor et al., Radar attenuation and temperature within the Greenland Ice Sheet, *J. Geophys. Res. Earth Surf.* **120**, 983–1008, (2015).
  40. P. W. Gorham et al., Measurements of the Suitability of Large Rock Salt Formations for Radio Detection of High Energy Neutrinos, *Nucl. Instrum. Meth.* **A490**, 476–491, (2002).
  41. A. Connolly et al., Measurements of radio propagation in rock salt for the detection of high-energy neutrinos, *Nucl. Instrum. Meth.* **A599**, 184–191, (2009).
  42. J. Alvarez-Muniz et al., Coherent radio pulses from showers in different media: A unified parameterization, *Phys. Rev. D*. **74**, 023007, (2006).
  43. G. R. Olohoeft and D. W. Strangway, Dielectric Properties of the First 100 Meters of the Moon, *Earth Planet Sci. Lett.* (1975).
  44. C. James, The lunar cherenkov technique - answering the unanswered questions, *Nucl. Instr. Meth.* **662**, S12–S19, (2012).
  45. P. W. Gorham et al., Experimental Limit on the Cosmic Diffuse Ultra-high Energy Neutrino Flux, *Phys. Rev. Lett.* **93**(4):041101, (2004).
  46. O. Scholten et al., Optimal radio window for the detection of ultra-high energy cosmic rays and neutrinos off the moon, *Astroparticle Physics*. **26**, 219, (2006).
  47. P. W. Gorham et al., The Antarctic Impulsive Transient Antenna Ultra-high Energy Neutrino Detector Design, Performance, and Sensitivity for 2006-2007 Balloon Flight, *Astropart. Phys.* **32**, 10–41, (2009).
  48. P. W. Gorham et al., The ExaVolt Antenna: A Large-Aperture, Balloon-embedded Antenna for Ultra-high Energy Particle Detection, *Astropart. Phys.* **35**, 242–256, (2011).
  49. C. W. James et al., Limit on UHE Neutrino Flux from the Parkes Lunar Radio Cherenkov Experiment, *Mon. Not. Roy. Astron. Soc.* **379**, 1037–1041, (2007).
  50. T. Miller, R. Schaefer, and H. B. Sequeira, PRIDE (Passive Radio [frequency] Ice Depth Experiment): An instrument to passively measure ice depth from a European orbiter using neutrinos, *Icarus*. **220**, 877–888, (2012).
  51. N. G. Lehtinen et al., FORTE satellite constraints on ultra-high energy cosmic particle fluxes, *Phys. Rev. D*. **69**, 013008, (2004).

52. J. D. Bray et al., A lunar radio experiment with the Parkes radio telescope for the LUNASKA project, *Astropart. Phys.* **65**, 22–39, (2014).
53. S. Hoover et al., Observation of Ultra-high-energy Cosmic Rays with the ANITA Balloon-borne Radio Interferometer, *Phys. Rev. Lett.* 105(15):151101, (2010).
54. P. Schellart et al., Detecting cosmic rays with the LOFAR radio telescope, *Astronomy and Astrophysics*. 560:A98, (2013).
55. O. Martineau-Huynh et al., Status of the TREND project. (2012). arXiv:1204.1559.
56. A. Aab et al., Energy Estimation of Cosmic Rays with the Engineering Radio Array of the Pierre Auger Observatory. (2015). arXiv:1508.04267.
57. O. Brusova et al. Radio Detection of Neutrinos from Behind a Mountain. In *Proceedings of the 30th International Cosmic Ray Conference*, vol. 5, pp. 1585–1588, (2008).
58. O. Martineau-Huynh et al. The Giant Radio Array for Neutrino Detection. In *European Physical Journal Web of Conferences*, vol. 116, p. 03005, (2016).
59. A. G. Viereg et al., The First Limits on the Ultra-high Energy Neutrino Fluence from Gamma-Ray Bursts, *ApJ*. 736:50, (2011).
60. H. Cathey, The NASA super pressure balloon - A path to flight, *Advances in Space Research*. **44**, 23–38, (2009).
61. F. . B. K. Baginski, Estimating the deployment pressure in pumpkin balloons, *AIAA Journal of Aircraft*. **48**, 235–247, (2011).
62. A. Romero-Wolf et al. The ExaVolt Antenna Mission Concept and Technology Developments. In *Proceedings of the 34th International Cosmic Ray Conference*, (2015).
63. P. Allison et al., Performance of two Askaryan Radio Array stations and first results in the search for ultra-high energy neutrinos. (2015). arXiv:1507.08991.
64. P. Allison et al., First Constraints on the Ultra-High Energy Neutrino Flux from a Prototype Station of the Askaryan Radio Array, *Astropart. Phys.* **70**, 62–80, (2015).
65. P. Allison et al., Constraints on the Ultra-High Energy Neutrino Flux from Gamma-Ray Bursts from a Prototype Station of the Askaryan Radio Array. (2015). arXiv:1507.00100.
66. S. W. Barwick et al., Design and Performance of the ARIANNA Hexagonal Radio Array Systems. (2014). arXiv:1410.7369.
67. F. Wu. *Using ANITA-I to constrain ultra high energy neutrino-nucleon cross section*. PhD thesis, University of California, Irvine, (2009).
68. S. A. Kleinfelder, Design and performance of the autonomous data acquisition system for the ARIANNA high energy neutrino detector, *IEEE Trans. Nucl. Sci.* **60**(2), 612–618, (2013).
69. S. W. Barwick et al. Livetime and sensitivity of the ARIANNA Hexagonal Radio Array. In *Proceedings of the 34th International Cosmic Ray Conference*, (2015).
70. S. W. Barwick et al., A First Search for Cosmogenic Neutrinos with the ARIANNA Hexagonal Radio Array, *Astropart. Phys.* **70**, 12–26, (2015).
71. R. B. Alley and B. R. Koci, Ice-core analysis at site A, Greenland: preliminary results, *Ann. Glaciol.* **10**, 14, (1988).
72. K. C. Kuivinen, A 237-meter ice core from South Pole Station, *Antarctic Journal of the United States*. **18**(5), 113–114, (1983).
73. J. D. Bray, The sensitivity of past and near-future lunar radio experiments to ultra-high-energy cosmic rays and neutrinos, *Astropart. Phys.* **77**, 1–20, (2016).
74. A. R. Beresnyak et al., Limits on the flux of ultra high-energy neutrinos from radio astronomical observations, *Astronomy Reports*. **49**, 127–133, (2005).
75. C. James et al., LUNASKA experiments using the Australia Telescope Compact Array to search for ultra-high energy neutrinos and develop technology for the lunar Cherenkov technique, *Phys. Rev. D*. **81**, 042003, (2010).

76. C. James. *Ultra-high energy particle detection with the lunar Cherenkov technique*. PhD thesis, The University of Adelaide, (2009).
77. T. R. Jaeger, R. L. Mutel, and K. G. Gayley, Project RESUN, a radio EVLA search for UHE neutrinos, *Astropart. Phys.* **34**, 293–303, (2010).
78. R. E. Spencer et al. La Luna: Lovell Attempts LUnar Neutrino Acquisition. In *10th European VLBI Network Symposium and EVN Users Meeting: VLBI and the New Generation of Radio Arrays*, p. 97, (2010).
79. J. D. Bray et al., Limit on the ultra-high-energy neutrino flux from lunar observations with the Parkes radio telescope, *Phys. Rev. D.* (2015).
80. J. D. Bray et al., Lunar detection of ultra-high-energy cosmic rays and neutrinos with the Square Kilometre Array. (2015). arXiv:1408.6069.
81. A. Romero-Wolf et al., An interferometric analysis method for radio impulses from ultra-high energy particle showers, *Astropart. Phys.* **60**, 72–85, (2015).
82. A. G. Viereg, K. Bechtol, and A. Romero-Wolf, A Technique for Detection of PeV Neutrinos Using a Phased Radio Array, *J. Cosm. and Astropart. Phys.* **1602**(02), 005, (2016).